23

A General Framework for Computation of Biomedical Image Moments

G.A. Papakostas, D.E. Koulouriotis, E.G. Karakasis and V.D. Tourassis
Democritus University of Thrace, Department of Production Engineering and Management
Greece

1. Introduction

Image moments have been successfully used as images' content descriptors for several decades. Their ability to fully describe an image by encoding its contents in a compact way makes them suitable in many disciplines of the engineering life, such as image analysis (Sim et al., 2004), image watermarking (Papakostas et al., 2010a) and pattern recognition (Papakostas et al., 2005, 2007, 2009a, 2010b). Apart from the *geometric moments*, which are firstly introduced, several moment types have been presented due time (Flusser et al., 2009).
Orthogonal moments are the most popular moments widely used in many applications owing to their orthogonality property that permits the reconstruction of the image by a finite set of its moments with minimum reconstruction error. This orthogonality property comes from the nature of the polynomials used as kernel functions, which they constitute an orthogonal base. As a result the orthogonal moments have minimum information redundancy meaning that different moment orders describe different image parts of the image. The most well known orthogonal moment families are: Zernike, Pseudo-Zernike, Legendre, Fourier-Mellin, Tchebichef, Krawtchouk, dual Hahn moments, with the last three ones belonging to the discrete type moments since they are defined directly to the image coordinate space, while the first ones are defined in the continue space.
Recently, there is an increased interest on applying image moments in biomedical imaging, with the reconstruction of medical images (Dai et al., 2010; Papakostas et al., 2009b; Shu et al., 2007; Wang & Sze, 2001) and the description of image's parts with particular properties (Bharathi & Ganesan, 2008; Iscan et al., 2010; Li & Meng, 2009; Liyun et al., 2009) by distinguishing diseased areas from the healthy ones, being the most active research directions the scientists work with.
Therefore, a method that computes fast and accurate the orthogonal moments of a biomedical image is of great importance. Although many algorithms and strategies (Papakostas et al., 2010c) have been proposed in the past, these methodologies handle the biomedical images as "every-day" images, meaning that they are not making use of specific properties of the image in process.
The authors have made a first attempt to compute the Krawtchouk moments of biomedical images by taking advantage of the inherent property of the biomedical image to have limited number of different intensity values (Papakostas et al., 2009c). Based on this observation and by applying the ISR method (Papakostas et al., 2008a) an image is

decomposed to a set of image slices consisting of pixels with the same intensity value, an image representation that enables the fast computation of the image moments (Papakostas et al., 2009d).
This first approach has shown very promising results, by giving more space to apply it to more moment families and biomedical datasets under a general framework, which is presented in this chapter.

2. Image moments

A general formulation of the $(n+m)^{th}$ order image moment of a NxN image with intensity function $f(x,y)$ is given as follows:

$$M_{nm} = NF \times \sum_{x=1}^{N} \sum_{y=1}^{N} Poly_n(x) Poly_m(y) f(x,y) \tag{1}$$

where NF is a normalization factor and $Poly_n(x)$ is the n^{th} order polynomial value of the pixel point with coordinate x, used as a moment kernel. According to the type of the polynomial kernel used in (1), the type of the moments is determined such as Geometric, Zernike, Pseudo-Zernike, Fourier-Mellin, Legendre, Tchebichef, Krawtchouk and dual Hahn.
For example, in the case of Tchebichef moments (Papakostas et al., 2009d, 2010c) the used polynomial has the form of the normalized Tchebichef polynomial defined as follows:

$$Poly_n(x) = \tilde{t}_n(x) = \frac{t_n(x)}{\beta(n,N)} \tag{2}$$

where

$$t_n(x) = (1-N)_n \, {}_3F_2(-n,-x,1+n;1,1-N;1) = \sum_{k=0}^{n} (-1)^{n-k} \binom{N-1-k}{n-k} \binom{n+k}{n} \binom{x}{k} \tag{3}$$

is the n^{th} order Tchebichef polynomial, ${}_3F_2$, the generalized hypergeometric function, $n,x = 0,1,2,\ldots,N-1$, N the image size and $\beta(n,N)$ a suitable constant independent of x that serves as scaling factor, such as N^n.
Moreover the normalization factor NF has the following form:

$$NF = \frac{1}{\tilde{\rho}(p,N)\tilde{\rho}(q,N)} \tag{4}$$

where $\tilde{\rho}(n,N)$ is the normalized norm of the polynomials

$$\tilde{\rho}(n,N) = \frac{\rho(n,N)}{\beta(n,N)^2} \tag{5}$$

with

$$\rho(n,N) = (2n)! \binom{N+n}{2n+1}, \quad n = 0,1,\ldots,N-1 \tag{6}$$

Based on the above assumptions, the final computational form of the $(n+m)^{th}$ order Tchebichef moments of a NxN image having $f(x,y)$ intensity function takes the following form:

$$T_{nm} = \frac{1}{\tilde{\rho}(n,N)\tilde{\rho}(m,N)} \sum_{x=0}^{N-1} \sum_{y=0}^{N-1} \tilde{t}_n(x)\tilde{t}_m(y) f(x,y) \tag{7}$$

Working in the same way, the computational formulas of Geometric, Zernike, Pseudo-Zernike, Legendre, Krawtchouk and dual Hahn moments can be derived (Papakostas et al., 2009d, 2010c) based on the general form of (1).

3. A general computation strategy

Generally, there are four main computation strategies (Papakostas et al., 2010c) that have been applied to accelerate the moments' computation speed: 1) the *Direct Strategy (DS)*, which firstly used, since it is based on the definition formulas of each moment family, 2) the *Recursive Strategy (RS)*, which is characterized by the mechanism of recursive computation of the kernel's polynomials, 3) the *Partitioning Strategy (PS),* according to which the image is partitioned into several smaller sub-images in order to reduce the maximum order need to computed and finally 4) the *Slice-Block Strategy (SBS)*, which decomposes a gray-scale image to intensity slices and rectangular blocks, developed by the authors (Papakostas et al., 2008a, 2009d).

Among the four above strategies the last one has the advantage to collaborate with the RS and PS strategies (Papakostas et al., 2010c), by resulting to more efficient computation schemes. Moreover, the SBS strategy can be applied to any moment family defined in the cartesian coordinate system (for the case of the polar coordinate system, appropriate transformation to the cartesian system is needed) in a common way, establishing it a general computation framework.

After the presentation of the main principles of the SBS methodology, this method will be applied to compute the moments of several families, for the case of biomedical images, which they constitute a special case of images where the benefits of the SBS strategy are significantly increased.

The principal mechanisms used by the SBS strategy are the *ISR (Image Slice Representation)* and *IBR (Image Block Representation)* methodologies, which decompose an image into intensity slices and a slice into rectangular blocks, respectively.

The main idea behind the ISR method is that we can consider a gray-scale image as the resultant of non-overlapped image slices, whose pixels have specific intensities. Based on this representation, we can decompose the original image into several slices, from which we can then reconstruct it, by applying fundamental mathematical operations.

Based on the above image decomposition, the following definition can be derived:

Definition 1: *Slice* of a gray-scale image, of a certain intensity f_i, is the image with the same size and the same pixels of intensity f_i as in the original one, while the rest of the pixels are considered to be black.

As a result of Definition 1, we derive the following Lemma 1 and 2:

Lemma 1: Any 8-bit gray-scale image can be decomposed into a maximum of 255 slices, where each slice has pixels of one intensity value and black.

Lemma 2: The binary image as a special case of a gray-scale image consists of only one slice, the binary slice, where only the intensities of 255 and 0 are included.

Based on the ISR representation, the intensity function *f(x,y)* of a gray-scale image can be defined as an expansion of the intensity functions of the slices:

$$f(x,y)=\sum_{i=1}^{s} f_i(x,y) \tag{8}$$

where s is the number of slices (equal to the number of different intensity values) and $f_i(x,y)$ is the intensity function of the i^{th} slice. In the case of a binary image s is 1 and thus $f(x,y)=f_1(x,y)$.

In the general case of gray-scale images, each of the extracted slices can be considered as a two-level image and thus the IBR algorithm (Papakostas et al., 2008a, 2009d) can be applied directly, in order to decompose each slice into a number of non-overlapped blocks.

By using the ISR representation scheme, the computation of the $(n+m)^{th}$ order orthogonal moment (1) of a gray-scale image $f(x,y)$, can be performed according to the equations

$$\begin{aligned} M_{nm} &= NF\times\sum_x\sum_y Poly_n(x)\,Poly_m(y)\,f(x,y) \\ &= NF\times\sum_x\sum_y Poly_n(x)\,Poly_m(y)\left(\sum_{i=1}^{s} f_i(x,y)\right) \\ &= NF\times\sum_x\sum_y Poly_n(x)\,Poly_m(y)\left(f_1(x,y)+f_2(x,y)+\ldots+f_s(x,y)\right)\Leftrightarrow \end{aligned} \tag{9}$$

$$\begin{aligned} M_{nm} &= NF\times\sum_x\sum_y Poly_n(x)\,Poly_m(y)f_1(x,y)+ \\ &\quad + NF\times\sum_x\sum_y Poly_n(x)\,Poly_m(y)f_2(x,y)+\ldots \\ &\quad + NF\times\sum_x\sum_y Poly_n(x)\,Poly_m(y)f_s(x,y) \\ &= f_1\left[NF\times\sum_{x_1}\sum_{y_1} Poly_n^1(x_1)\,Poly_m^1(y_1)\right]+ \\ &\quad + f_2\left[NF\times\sum_{x_2}\sum_{y_2} Poly_n^2(x_2)\,Poly_m^2(y_2)\right]+\ldots \\ &\quad + f_s\left[\sum_{x_s}\sum_{y_s} Poly_n^s(x_n)\,Poly_m^s(y_n)\right] \\ &= f_1M_{nm}^1+f_2M_{nm}^2+\ldots+f_sM_{nm}^s \end{aligned} \tag{10}$$

where f_i and M_{nm}^i, $i=1,2,\ldots,s$ are the intensity functions of the slices and the corresponding $(n+m)^{th}$ order moments of the i^{th} binary slice, respectively.

The corresponding moment of a binary slice M_{nm}^i is the moment computed by considering a block representation of the image (Papakostas et al., 2008a, 2009d), as follows:

$$M_{nm}^{i}=\sum_{j=0}^{k-1}M_{nm}\left(b_j\right)=\sum_{j=0}^{k-1}\sum_{x=x_{1,b_j}}^{x_{2,b_j}}\sum_{y=y_{1,b_j}}^{y_{2,b_j}}Poly_n(x)Poly_m(y)$$
$$=\sum_{j=0}^{k-1}\left(\sum_{x=x_{1,b_j}}^{x_{2,b_j}}Poly_n(x)\right)\left(\sum_{y=y_{1,b_j}}^{y_{2,b_j}}Poly_m(y)\right) \quad (11)$$

where x_{1,b_j}, x_{2,b_j} and y_{1,b_j}, y_{2,b_j} are the coordinates of the block b_j, with respect to the horizontal and vertical axes, respectively.

A result of the above analysis (10) is the following Proposition 1:

Proposition 1: The *(n+m)th* order discrete orthogonal moment of a gray-scale image is equal to the "intensity-weighted" sum of the same order discrete orthogonal moments of a number of binary slices.

The SBS strategy has been applied successfully in computing the geometric moments (Papakostas et al., 2008a), the orthogonal moments (Papakostas et al., 2009d) and the DCT (Papakostas et al., 2008b, 2009e), by converging to high computation speeds in all the cases.

The performance of the SBS methodology is expected to be higher for the case of the biomedical images, since the limited number of different intensities of these images, enables the construction of less intensity slices and therefore bigger homogenous rectangular blocks are extracted.

4. Biomedical images – A special case

As it has already been mentioned in the previous sections, the application of the SBS strategy can significantly increases the moments' computation rate for the case of biomedical images, as compared with the "every-day" images. This is due to the fact that the biomedical images are "intensity limited" since the pixels' intensities are concentrated mostly in a few intensity values. For example, let see the two "every-day" images Lena and Barbara as illustrated in the following Fig. 1, along with their corresponding histograms.

These images having a content of general interest, present a more normally distributed pixel's intensities into the intensity range [0-255].

On the contrary, in the case of biomedical images the intensities are concentrated in a narrower region of the intensity range. Figure 2, shows four sample images from three different kinds of biomedical images BRAINX, KNIX (MRI images), INCISIX (CT images) retrieved from (DICOM) and MIAS (X-ray images) (Suckling et al., 1994). All the images have 256x256 pixels size, while each dataset consists of 232 (BRAINIX), 135 (KNIX), 126 (INCISIX), 322 (MIAS) gray-scale images.

It is noted that in the above histograms the score of the 0 intensity is omitted for representation purposes, since a lot of pixels have this intensity value, causing the covering of all the other intensity distributions.

A careful study of the above histograms can lead to the deduction that the most pixels' intensities are limited to a small fraction of the overall intensity range [0-255]. This means that the images' content is concentrated in a few intensity slices. This fact seems to be relative to the images' nature and constitutes an inherent property of their morphology. From (10) and (11) it is obvious that the performance of the SBS method is highly dependent on the image's intensity distribution, meaning that images with less intensities and big

blocks enable the achievement of high moments' computation rates, conditions that are satisfied by the biomedical images.

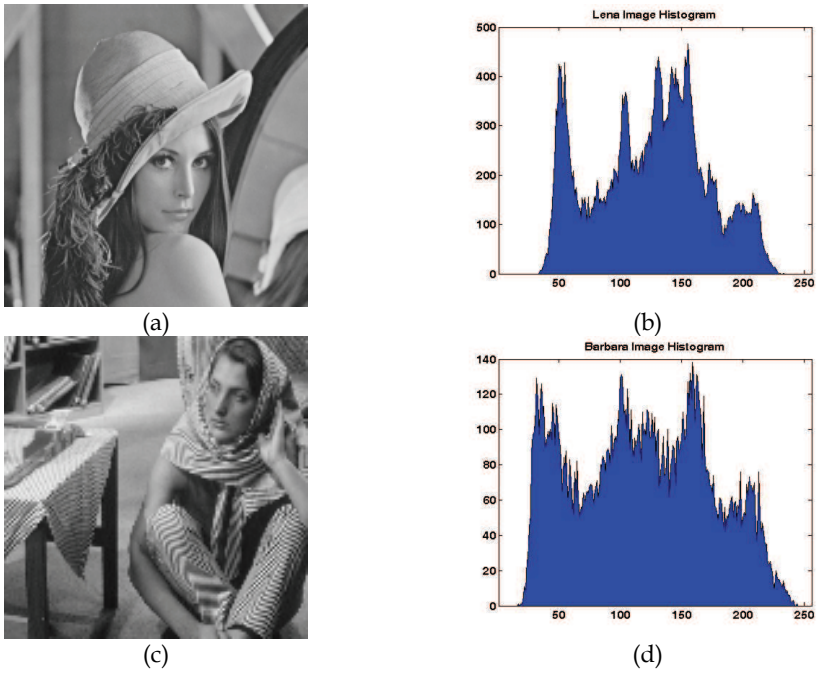

Fig. 1. "Every-day" images and their histograms: (a)–(b)Lena image and its histogram, (c)-(d) Barbara image and its histogram.

5. Experimental study

In order to investigate the performance of the SBS strategy in computing the biomedical image moments, a set of experiments have been arranged. For this reason five representative moment families the *Geometric Moments (GMs), Legendre Moments (LMs), Tchebichef Moments (TMs), Krawtchouk Moments (KMs)* and *dual Hahn Moments (DHMs)*, are computed to the entire four datasets of Fig.2, up to a maximum order from 0 to 50 with step 5. The variance (σ) and mean (μ) values of the SBS strategy results are summarized in the following Table 1.

	BRAINIX	**KNIX**	**INCISIX**	**MIAS**
Block Extraction Time(msecs)	0.0234/1.1117	0.1189/1.8363	0.0874/1.9470	0.0442/0.9915
Num. of Blocks	1.7477E+07/28325	4.6382E+07/48291	2.3089E+06/56265	3.7785E+07/22053
Num. of Intensity Slices	740.1785/213.7845	305.7875/231.5407	136.3860/241.7169	220.6238/237.5280

Table 1. Performance statistics (σ/μ) of applying SBS to the datasets.

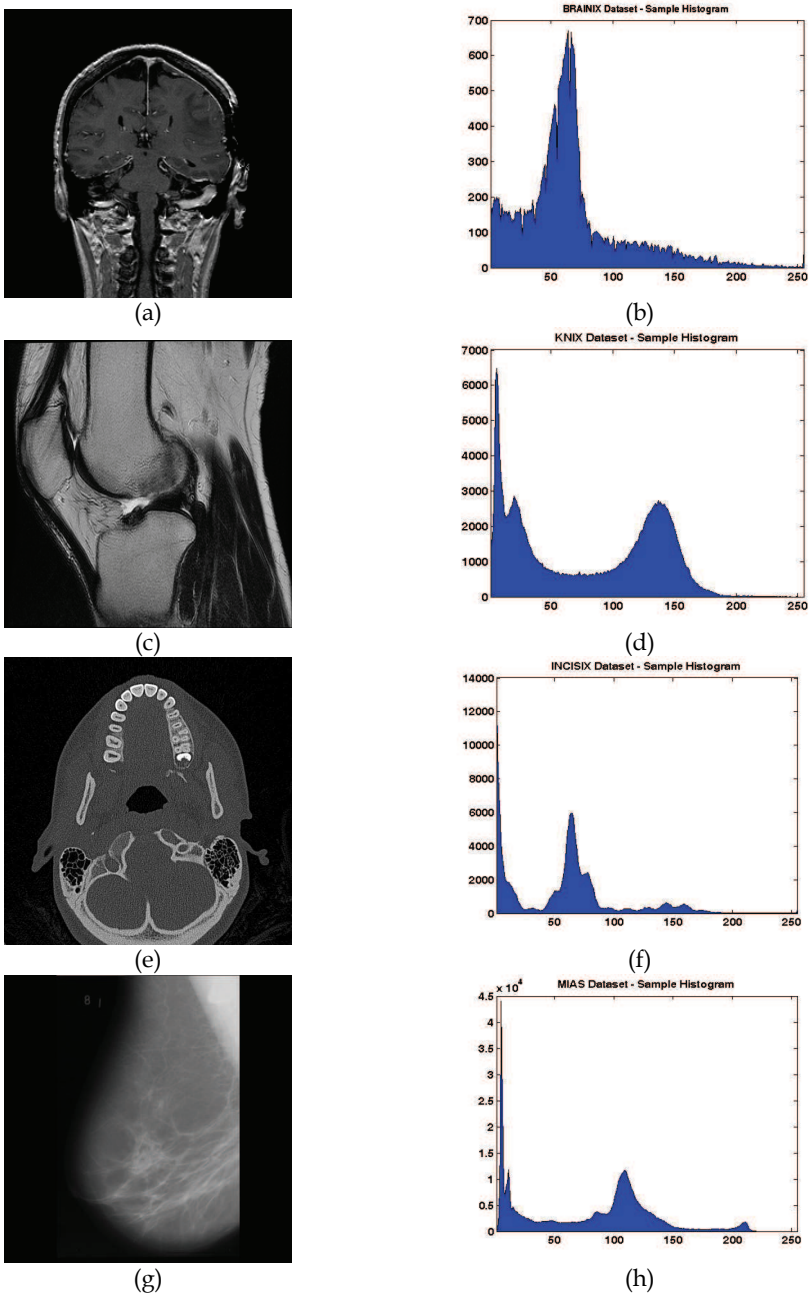

Fig. 2. Biomedical images and their histograms: (a)-(b) BRAINIX sample image and its histogram, (c)-(d) KNIX sample image and its histogram, (e)-(f) INCISIX sample image and its histogram, (g)-(h) MIAS sample image and its histogram.

From the above results, it can be realized that the extraction of the homogenous block does not add a significant overhead to the entire computation procedure (small mean values with low variability), since it needs a little time to be executed. On the other hand, the high variance on the number of blocks and intensity slices, reveal a complicated dependency of the computation time on these two main factors, as far as the size of the blocks and the distribution of the blocks on the intensity slices are concerned.
In order to study the timing performance of the SBS strategy, a comparison of its behaviour with that of the DS methodology, for the case of the four biomedical datasets has been taken place. Since, the SBS strategy can effectively be collaborated with other fast strategies (RS and PS) (Papakostas et al., 2010c), only a comparison with the DS methodology is needed to highlight its advantages. The mean values of the computation time in each case are illustrated in the following Table 2, 3 and 4. From these results it is obvious that the proposed method needs less time to compute the moments of any order, as compared to the DS one. This outperformance varies by the moment family, since each family needs a different time to compute its moments.

Order	**Moment Families (BRAINIX Dataset)**									
	GMs		**LMs**		**TMs**		**KMs**		**DHMs**	
	DS	*SBS*	*DS*	*SBS*	*DS*	*SBS*	*DS*	*SBS*	*DS*	*SBS*
0	15	9	4	2	23	14	198	125	11775	7207
5	554	349	3452	2110	2352	1455	7663	4864	713050	436919
10	1877	1185	14611	8929	15087	9348	28091	17814	2617380	1601577
15	3955	2493	36663	22446	47139	29211	64455	40764	5716791	3497941
20	6808	4289	72640	44454	108589	67167	119837	75595	10037777	6142626
25	10441	6573	125502	76874	208647	128912	196699	123978	15590386	9541093
30	14844	9339	200755	122885	355676	219857	298193	187821	22386172	13700734
35	19980	12567	298700	183023	556002	343423	426135	268199	30487995	18667254
40	25843	16266	423570	259605	825554	509665	584561	367523	39895856	24423207
45	32487	20465	577570	354053	1168458	720985	774426	486405	50549799	30948566
50	39909	25147	767700	470815	1598002	988073	1000782	627991	62496927	38267424

Table 2. Timing performance (msecs) for the case of BRAINIX dataset.

Order	**Moment Families (KNIX Dataset)**									
	GMs		**LMs**		**TMs**		**KMs**		**DHMs**	
	DS	*SBS*	*DS*	*SBS*	*DS*	*SBS*	*DS*	*SBS*	*DS*	*SBS*
0	13	11	4	3	25	21	200	171	11762	9975
5	508	443	3261	2746	2455	2082	7820	6697	708705	601321
10	1720	1501	14204	11950	15517	13143	28786	24624	2598280	2204667
15	3824	3346	36354	30605	48075	40717	65699	56164	5693130	4831323
20	6623	5799	72407	60926	110151	93218	121549	103819	9999761	8486341
25	10108	8851	125500	105649	209637	177333	199574	170328	15565313	13211695
30	14233	12461	200015	168363	355661	300744	302023	257620	22380144	18996004
35	19047	16675	296031	249264	555787	469906	431928	368258	30466446	25858760
40	24590	21519	420693	354320	823488	696162	592365	504798	39823488	33801678
45	30806	26959	574196	483628	1170698	989141	783864	667674	50473687	42842306
50	37735	33021	759956	640210	1605292	1355880	1012044	861656	62430595	52992467

Table 3. Timing performance (msecs) for the case of KNIX dataset.

Order	Moment Families (INCISIX Dataset)									
	GMs		LMs		TMs		KMs		DHMs	
	DS	*SBS*	*DS*	*SBS*	*DS*	*SBS*	*DS*	*SBS*	*DS*	*SBS*
0	13	12	4	4	32	30	201	188	11922	11145
5	496	475	3578	3338	3272	3050	7783	7275	722863	675832
10	1685	1614	15295	14254	20771	19302	28372	26505	2660991	2487824
15	3572	3422	38163	35545	67594	62776	70776	66143	5864036	5482582
20	6188	5929	75896	70658	153916	143171	138969	129886	10284282	9615163
25	9475	9078	131719	122599	266591	247966	235428	220038	15971863	14932422
30	13464	12904	208231	193770	425457	395679	359150	335315	22919177	21427273
35	18187	17431	322708	300266	671490	624761	522587	487417	31164529	29135577
40	23591	22614	504327	469081	983175	914848	706469	658649	40724145	38072365
45	29692	28472	726877	675879	1346551	1252703	913268	851339	51649763	48285960
50	36558	35077	932814	867355	1816793	1690125	1156850	1078288	63889158	59727774

Table 4. Timing performance (msecs) for the case of INCISIX dataset.

Order	Moment Families (MIAS Dataset)									
	GMs		LMs		TMs		KMs		DHMs	
	DS	*SBS*	*DS*	*SBS*	*DS*	*SBS*	*DS*	*SBS*	*DS*	*SBS*
0	13	6	4	2	24	11	197	89	11835	4809
5	509	240	3333	1522	2398	1099	7856	3571	710597	290989
10	1714	809	14452	6593	15442	7091	28732	13070	2609070	1067752
15	3623	1712	36858	16863	48365	22174	65639	29875	5710608	2337811
20	6272	2964	73305	33510	110365	50572	121797	55539	10042048	4113727
25	9628	4550	127805	58579	209384	96111	199562	90988	15602271	6392757
30	13653	6456	202445	92886	355803	163355	301687	137453	22409641	9184141
35	18387	8697	300303	137786	557843	256311	431414	196660	30481570	1249575
40	23830	1274	425532	195223	824113	378585	590462	269338	39851184	1634314
45	29986	4187	581006	266380	1162588	534107	783667	357651	50506603	2072049
50	36819	7432	770337	353421	1584871	728010	1012265	461968	62485283	2564557

Table 5. Timing performance (msecs) for the case of MIAS dataset.

A more descriptive way to present the performance of the SBS methodology is by computing the *Computation Time Reduction (CTR)*, defined in the following equation (12) and depicted in Fig.3 for the case of all moment families and biomedical image datasets.

$$CTR-\% \ = \frac{Time^{DS} - Time^{SBS}}{Time^{DS}} \times 100 \tag{12}$$

The above diagrams clearly show that the reduction of the computation time by using the SBS strategy is significant for all the cases. More precisely, this reduction varies between 37%-50%, 12%-25%,0%-7.5% and 50%-95% for the BRAINX, KNIX, INCISIX and MIAS datasets respectively. This diversity of the reduction owing to the different intensity distribution each image dataset presents, forming different number of blocks as shown in Table 1.

Another important outcome from the above plots is that all the moment families give near the same reduction for the same dataset and moreover this reduction is quite stable as the moment order increases (DHMs constitutes an exception for the case of MIAs dataset, where

the reduction is significant higher (95%), for the high moment orders, as compared with the rest moment families (58%)).

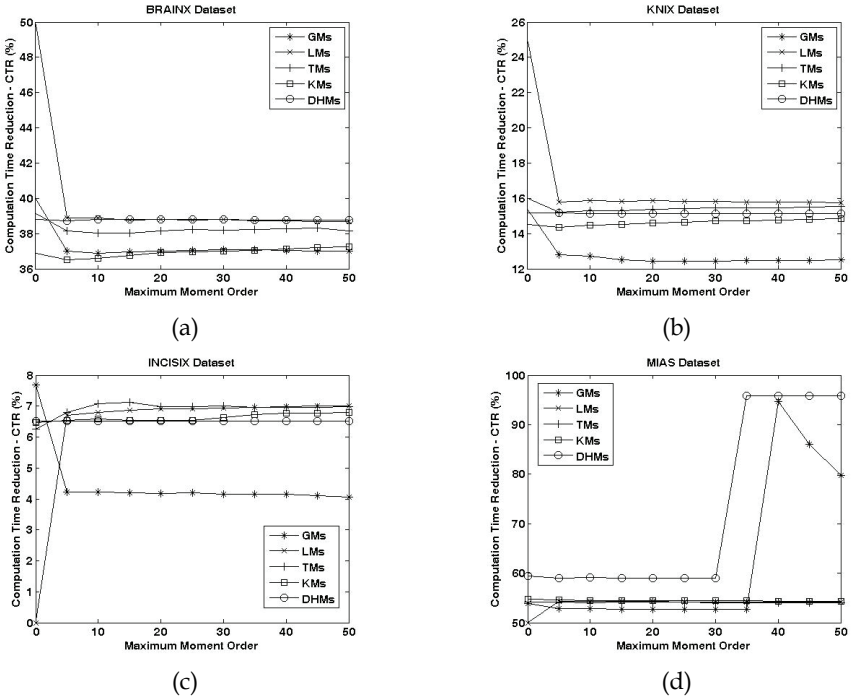

Fig. 3. Computation time reduction for the case of (a) BRAINIX, (b) KNIX, (c) INCISIX and (d) MIAS, datasets.

6. Conclusion

A morphology-driven methodology that improves the computation rates of the biomedical image moments was presented and analyzed in the previous sections. The usage of the introduced methodology can reduce the computation overhead by a significant factor depending on the image intensity morphology. This improvement is mainly achieved due to the biomedical images' nature dealing with their intensities distribution, which boosts the performance of the proposed computation scheme.

7. References

Bharathi, V.S. & Ganesan, L. (2008). Orthogonal moments based texture analysis of CT liver images. *Pattern Recognition Letters*, Vol. 29, No. 13, pp. 1868-1872.

Dai, X.B.; Shu, H.Z.; Luo, L.M.; Han, G.N. & Coatrieux, J.L. (2010). Reconstruction of tomographic images from limited range projections using discrete Radon transform and Tchebichef moments. *Pattern Recognition*, Vol. 43, No. 3, pp. 1152-1164.

DICOM, Retreived 16/08/2010 from http://pubimage.hcuge.ch:8080/.

Flusser, J.; Suk, T. & Zitova, B. (2009). *Moments and Moment Invariants in Pattern Recognition*. Wiley. Chichester.

Iscan, Z.; Dokur, Z. & Ölmez, T. (2010). Tumor detection by using Zernike moments on segmented magnetic resonance brain images. *Expert Systems with Applications*, Vol. 37, No. 3, pp.2540-2549.

Suckling, J et al (1994) "The Mammographic Image analysis society digital mammogram database. *Exerpta Medica. International Congress Series* 1069, pp. 375-378.

Li, B. & Meng, M.Q.-H. (2009). Computer-based detection of bleeding and ulcer in wireless capsule endoscopy images by chromaticity moments. *Computers in Biology and Medicine*, Vol. 39, No. 2, pp. 141-147.

Liyun, W.; Hefei, L.; Fuhao, Z.; Zhengding, L. & Zhendi, W. (2009). Spermatogonium image recognition using Zernike moments. *Computer Methods and Programs in Biomedicine*, Vol. 95, No. 1, pp. 10-22.

Papakostas, G.A.; Karras, D.A.; Mertzios, B.G. & Boutalis, Y.S. (2005). An efficient feature extraction methodology for computer vision applications using wavelet compressed Zernike moments", *ICGST International Journal on Graphics, Vision and Image Processing, Special Issue: Wavelets and Their Applications*, Vol. SI1, pp. 5-15.

Papakostas, G.A.; Boutalis, Y.S.; Karras, D.A. & Mertzios, B.G. (2007). "A new class of Zernike moments for computer vision applications. *Information Sciences*, Vol. 177, No.13, pp. 2802-2819.

Papakostas, G.A.; Karakasis, E.G. & Koulouriotis, D.E. (2008). Efficient and accurate computation of geometric moments on gray-scale images. *Pattern Recognition*, Vol. 41, No. 6, pp. 1895-1904.

Papakostas, G.A.; Karakasis, E.G. & Koulouriotis, D.E. (2008b). On accelerating the computation of 2-D discrete cosine transform in image processing. *International Conference on Signals and Electronic Systems (ICSES'08)*, *(IEEE Xplore)*, pp. 7-10, Krakow – Poland.

Papakostas, G.A.; Boutalis, Y.S.; Karras, D.A. & Mertzios, B.G. (2009a). Pattern classification by using improved wavelet compressed Zernike moments. *Applied Mathematics and Computation*, Vol. 212, No. 1, pp. 162-176.

Papakostas, G.A.; Karras, D.A. & Mertzios, B.G. (2009b). Performance of the orthogonal moments in reconstructing biomedical images. *Proceedings of 16th International Workshop on Systems, Signals and Image Processing (IWSSIP'09)*, *(IEEE Xplore)*, pp. 1-4, Chalkida – Greece.

Papakostas, G.A.; Karakasis, E.G. & Koulouriotis, D.E. (2009c). Computing orthogonal moments in biomedical imaging. *Proceedings of 16th International Workshop on Systems, Signals and Image Processing (IWSSIP'09)*, *(IEEE Xplore)*, pp. 1-4, Chalkida – Greece.

Papakostas, G.A.; Koulouriotis, D.E. & Karakasis, E.G. (2009d). A unified methodology for efficient computation of discrete orthogonal image moments. *Information Sciences*, Vol. 179, No. 20, pp. 3619-3633.

Papakostas, G.A.; Koulouriotis, D.E. & Karakasis, E.G. (2009e). Efficient 2-D DCT computation from an image representation point of view", pp. 21-34, *Image Processing*, InTech.

Papakostas, G.A.; Tsougenis, E.D. & Koulouriotis, D.E. (2010a). Near optimum local image watermarking using Krawtchouk moments", *IEEE International Workshop on Imaging Systems and Techniques (IST'10),* pp. 459-462, Thessaloniki – Greece.

Papakostas, G.A.; Karakasis, E.G. & Koulouriotis, D.E. (2010b). Novel moment invariants for improved classification performance in computer vision applications. *Pattern Recognition*, Vol. 43, No. 1, pp. 58-68.

Papakostas, G.A.; Koulouriotis, D.E. & Karakasis, E.G. (2010c). Computation strategies of orthogonal image moments: a comparative study. *Applied Mathematics and Computation*, Vol. 216, No. 1, pp. 1-17.

Shu, H.Z.; Zhou, J.; Han, G.N.; Luo, L.M. & Coatrieux, J.L. (2007). Image reconstruction from limited range projections using orthogonal moments. *Pattern Recognition*, Vol. 40, No. 2, pp. 670-680.

Sim, D.G.; Kim, H.K. & Park, R.H. (2004). Invariant texture retrieval using modified Zernike moments. *Image and Vision Computing*, Vol. 22, No. 4, pp. 331-342.

Wang, T.J. & Sze, T.W. (2001). The image moment method for the limited range CT image reconstruction and pattern recognition. *Pattern Recognition*, Vol. 34, No. 11, pp. 2145-2154

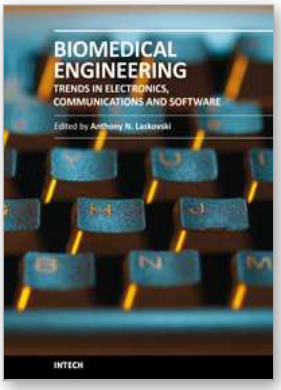

Biomedical Engineering, Trends in Electronics, Communications and Software

Edited by Mr Anthony Laskovski

ISBN 978-953-307-475-7
Hard cover, 736 pages
Publisher InTech
Published online 08, January, 2011
Published in print edition January, 2011

Rapid technological developments in the last century have brought the field of biomedical engineering into a totally new realm. Breakthroughs in materials science, imaging, electronics and, more recently, the information age have improved our understanding of the human body. As a result, the field of biomedical engineering is thriving, with innovations that aim to improve the quality and reduce the cost of medical care. This book is the first in a series of three that will present recent trends in biomedical engineering, with a particular focus on applications in electronics and communications. More specifically: wireless monitoring, sensors, medical imaging and the management of medical information are covered, among other subjects.

How to reference

In order to correctly reference this scholarly work, feel free to copy and paste the following:

G.A. Papakostas, D.E. Koulouriotis, E.G. Karakasis and V.D. Tourassis (2011). A General Framework for Computation of Biomedical Image Moments, Biomedical Engineering, Trends in Electronics, Communications and Software, Mr Anthony Laskovski (Ed.), ISBN: 978-953-307-475-7, InTech, Available from: http://www.intechopen.com/books/biomedical-engineering-trends-in-electronics-communications-and-software/a-general-framework-for-computation-of-biomedical-image-moments

INTECH
open science | open minds

InTech Europe
University Campus STeP Ri
Slavka Krautzeka 83/A
51000 Rijeka, Croatia
Phone: +385 (51) 770 447
Fax: +385 (51) 686 166
www.intechopen.com

InTech China
Unit 405, Office Block, Hotel Equatorial Shanghai
No.65, Yan An Road (West), Shanghai, 200040, China
中国上海市延安西路65号上海国际贵都大饭店办公楼405单元
Phone: +86-21-62489820
Fax: +86-21-62489821